


Article

Numerical Computation of Hybrid Morphologies of Nanoparticles on the Dynamic of Nanofluid: The Case of Blood-Based Fluid

Meznah M. Alanazi ¹, Awatif A. Hendi ¹, Qadeer Raza ², Muhammad Abdul Rehman ³,
Muhammad Zubair Akbar Qureshi ³, Bagh Ali ^{2,4,*}  and Nehad Ali Shah ^{5,*}

¹ Department of Physics, College of Science, Princess Nourah bint Abdulrahman University, P.O. Box 84428, Riyadh 11671, Saudi Arabia

² Department of Applied Mathematics, Northwestern Polytechnical University, Dongxiang Road, Beilin District, Xi'an 710129, China

³ Department of Mathematics, Air University Islamabad, Multan 60000, Pakistan

⁴ Faculty of Computer Science and Information Technology, Superior University, Lahore 54000, Pakistan

⁵ Department of Mechanical Engineering, Sejong University, Seoul 05006, Republic of Korea

* Correspondence: baghalisewag@mail.nwpu.edu.cn (B.A.); nehadali199@sejong.ac.kr (N.A.S.)

Abstract: The movement of biological fluids in the human body is a premium field of interest to overcome growing biomedical challenges. Blood behavior shows different behavior in capillaries, veins, and arteries during circulation. In this paper, a new mathematical relation for the nano-layer of biological fluids flows with the effect of TiO₂ and Ag hybrid nanoparticles was developed. Further, we explain the engineering phenomena of biological fluids and the role of hybrid nanoparticles in the blood vessel system. The improvement of drug delivery systems by using low seepage Reynolds number was associated with expansion/contraction and was discussed in detail through the rectangular domain. Using similarity transformation, the governing equations were converted into non-linear ordinary differential equations, and the mathematical problem was solved by employing the numerical shooting method. Plots of momentum, temperature, skin friction coefficient, as well as the Nusselt number on different non-dimensionless parameters are displayed via lower/upper porous walls of the channel. It was analyzed that the walls of the channel showed different results on magnetized physical parameters. Values of thermophoresis and the Brownian motion flow of the heat transfer rate gradually increased on the upper wall and decreased on the lower wall of the channel. The important thing is that the hybrid nanoparticles, rather than nano, were more useful for improving thermal conductivity, heat transfer rate, and the nano-layer.

Keywords: hybrid nanofluids; blood vessels system; thermophysical properties; biological fluids

MSC: 35Q30; 76D05; 76R10



Citation: Alanazi, M.M.; Hendi, A.A.; Raza, Q.; Rehman, M.A.; Qureshi, M.Z.A.; Ali, B.; Shah, N.A. Numerical Computation of Hybrid Morphologies of Nanoparticles on the Dynamic of Nanofluid: The Case of Blood-Based Fluid. *Axioms* **2023**, *12*, 163. <https://doi.org/10.3390/axioms12020163>

Academic Editors:
Francesco dell'Isola,
Hovik Matevosian and
Giorgio Nardo

Received: 8 December 2022

Revised: 30 January 2023

Accepted: 30 January 2023

Published: 6 February 2023



Copyright: © 2023 by the authors. Licensee MDPI, Basel, Switzerland. This article is an open access article distributed under the terms and conditions of the Creative Commons Attribution (CC BY) license (<https://creativecommons.org/licenses/by/4.0/>).

1. Introduction

The study related to the flow of nanofluids through deformable porous domains such as channels or pipes has appealed to the attention of many research groups because it plays a key role in illustrating numerous engineering phenomena related to various industrial and biological problems. Porous domains were utilized earlier for the illustration of many surface mechanisms such as propellant burning, uniformly distributed irrigation, natural transpiration, drug delivery system, natural transpiration, ablation cooling, and phase sublimation. Majdalani et al. [1] determined that biological fluid movement through contracting or expanding vasculature is characterized by little seepage. The current work concentrates on the viscous flow caused by tiny wall contractions and expansions of two weakly permeable walls. Heat transport and unstable oscillatory flow in a horizontal composite porous media were studied by Umavathi et al. [2]. The pioneering work by Choi

in 1995 [3] for the enhancement of heat and mass transfer has proven to be a game-changer in the field of thermodynamics and fluid mechanics. The use of nanoparticles instead of microparticles for the production of heat transfer fluids not only removed the barriers from the way of heat transfer observed in the case of conventional fluids and macro-fluids, such as the rapid settlement of particles and limited heat transfer, but they are also favorable due to their applicable uplifted thermophysical properties, higher stability [4], and diverse applications in major technological and biomedical engineering fields. Hybrid nanofluids are formed by suspending more than one distinct nanoparticle in the base fluid. The development of hybrid nanofluids is a compromise between the benefits and drawbacks [5]. Sarkar et al. [6] declared that the hybrid nanofluids attained much attention due to their simultaneous combination of physical as well as chemical properties, which is simply a suspension of two different materials in a single base fluid for feasible applications, where mono-particle nanofluids can play a vital role or fulfill the specific requirements. The major factors that affect the selection of nanomaterials for hybrid nanofluids are availability, stability, toxicity, thermophysical properties, compatibility with the base fluid, inter-compatibility of both nanomaterials, and preparation cost [7]. Numerous studies have revealed the superior heat transfer characteristics of hybrid nanofluids, but the stability issues and dispersion of suspended particles in the base fluids are the two major worries that need to be resolved as early as possible for practical applications [8]. Hybrid nanofluids are relatively low-cost, efficient, and have tunable characteristics [9].

After the pioneering work on nanofluids by Choi and Eastman, plenty of research reports have been submitted related to the behavior of various nanofluids in various mediums [10]. A plethora of research reports can be found related to water, ethylene glycol, and oil-based mono-particle as well as hybrid nanofluids [11], but very few reports can be found about the thermo-physical features of bio-fluid-based hybrid nanofluids. Yurong et al. [12] studied the heat transfer characteristics of TiO_2 nanoparticles in water flowing in a vertical flow channel in the upward direction. Li et al. [13] computationally analyzed the nanofluid flow in microchannels for their prime application in micro-heat sinks and bio-MEMS. Mishra et al. [14] investigated the optical properties of gold nanoparticle biological nanofluids (vinyl pyrrolidone). Bajestan et al. [15] conducted experimental as well as numerical studies of nanofluids for their use in solar heat exchangers. In 2018, Ali et al. [16] discussed preparation techniques for TiO_2 , its applications, and major hurdles in the way of advanced research of nanofluids. Dakshayani et al. [17] analyzed the anticoagulant, antimicrobial, and antiplatelet characteristics of green synthesized silver nanoparticles with the help of *Selaginella* extract. Brzóška et al. [18] organized the sustainable heat transfer media with higher thermal conductivity by using multiwall carbon nanotubes in the bio-based fluids for the development of green bio-based nanofluids.

Following the concept of nanofluids, in 2007, Jana et al. [19] compared the elevation of heat transfer rate with the use of one and more than one nanoparticle in the base fluids. This was the first time hybrid nanofluids were kept into account. In that manuscript, Cu, Au, CNT mono-particle nanofluids, Cu-CNT, and Au-CNT hybrid nanofluids were considered. The Cu-nanofluid was the most efficient one, and the hybrid nanofluids were less efficient compared to the Cu-nanofluid. After that, numerous experiments and computational studies were conducted to assess the thermo-physical traits of various hybrid nanofluids. By most literature surveys, it was observed that efficiency depends upon the suspended nanoparticles (mono-nanoparticles and hybrid nanoparticles) as well as on the base fluid [20]. Madhesh et al. [21] investigated the convective heat transfer of Cu- TiO_2 hybrid nanofluids in a tube-like container for heat exchangers. The enhancement of the heat transfer rate was witnessed by increasing the volume concentration of copper-titania hybrid nanoparticles. Sundar et al. [22] elaborated on the superior heat transfer rate and friction factor of multiwall carbon nanotube (MWCNT)- Fe_3O_4 aqueous hybrid nanofluids. Dinarvand et al. [23] worked on the impact of CuO-Cu in blood hybrid nanofluid flowing in the micro-circulatory system on the drug delivery system. Later on, Chahregh and Dinarvand [24] formulated the model to study the behavior of Ag- TiO_2 hybrid nanoparticles

in the blood circulatory system in the large arteries where blood behaves as Newtonian. Their study mainly focused on drug delivery applications for the respiratory system. The experimental investigation and mathematical computation of heat transfer and the friction factor of $\text{TiO}_2\text{-SiO}_2$ hybrid nanoparticles in ethylene glycol and water were considered by Ramadhan and his coworkers [25]. Kim et al. [26] proposed gold and silver hybrid nanoparticles as the prime candidate for a cure for bacterial infection. Furthermore, they explained their vital role in photo-acoustic imaging for diagnostic purposes. An examination by Rathore [27] was conducted to evaluate the heat transfer in blood flowing through the stenotic artery while it is suspended in $\text{GO-Al}_2\text{O}_3$. Radiative heat, a constant magnetic field, dissipative, and Cattaneo-Christov thermal flux effects are all present in the 2D hybrid blood flow. A 2D computational analysis of hybridized ferrofluid for enhanced heat transport in MHD flow generated by elongating surfaces with radiation impact was investigated by Sandeep et al. [28]. Rathore et al. [29] evaluated the impact of resistive and radiative heat on graphene oxide (GO) and titanium dioxide (TiO_2) suspended Sutter by blood flow through the stenosed artery. Using a container with changing parameters, Riahi et al. [30] discussed the discretization of nanofluid convective movement using finite elements. Focusing on the three-dimensional (3D) Casson nanofluid flow over a narrowing sheet in porous layers, Durgaprasad et al. [31] took into account thermophoresis and the Brownian motion phenomenon. A study by Wakif et al. [32] considered a meta-analysis on the relevance of nano or small particles subjected to thermophoretic force due to temperature differential during the dynamics of liquid substances. Amidu et al. [33] obtained qualitative results toward understanding the influence of various slip mechanisms on the natural heat transfer performance of nanofluids. In this study, sedimentation, Brownian diffusion, and thermophoretic diffusion were all taken into account as slide processes.

After surveying most of the available literature, we found that there are some reports related to $\text{TiO}_2\text{-Ag}$ nanoparticles suspended in Newtonian blood flow in large arteries. However, no one ever reported the thermo-physical properties of $\text{TiO}_2\text{-Ag}$ hybrid nanoparticles in small arteries where blood behaves as a non-Newtonian fluid. Motivated by the wide scope of nanofluid application, we considered the current elaborated fluid problem. The primary aim of this study was to show the influence of hybrid nanoparticles on the dynamics of a Casson hybrid nanofluid subjected to two parallel plates. The above available studies showed that less consideration is given to this study, and this report will be very useful for experts to explore various features and to analyze the different outcomes. We focused on the comparison of the thermo-physical properties of mono-particle nanofluids ($\text{TiO}_2/\text{Blood}$ and Ag/Blood) and the hybrid nanofluid ($\text{TiO}_2\text{-Ag}/\text{Blood}$).

2. Mathematical Formulation

Blood exhibits Newtonian and non-Newtonian type fluids in nature depending on the size of the artery, which is significantly attractive for diverse research purposes in biomedical engineering and drug delivery. Blood behaves as Newtonian fluid in large arteries, while on the other hand, the non-Newtonian behavior is more significant in narrow blood vessels [34]. Due to this specific behavior of blood, it can be referred to as Casson fluid. Casson fluids behave like a fluid when suitable shear stress is applied; otherwise, they behave as a solid [35]. For better blood circulation, it is mandatory to maintain the standard viscosity as well as the temperature of the blood. To modify the thermophysical properties of blood, hybrid nanoparticles are dispersed in the blood to improve the thermophysical of blood [36]. Considering the laminar, incompressible, isothermal, and two-dimensional non-Newtonian Casson hybrid nanofluid ($\text{TiO}_2\text{-Ag}/\text{blood}$) flow in the rectangular domain by two porous surfaces, this enables the fluid to enter or exit during successive expansion or contraction and can be proven as the most appropriate prototype for hydrodynamic/thermal analysis of arterial blood flow. The geometry is created through substantial alteration [37]. Both walls have the same permeability and are capable of moving up and down at a time-dependent rate of $a'(t)$ with a distance of $2a(t)$. The temperature at the lower and upper walls of the channel are represented by the parameters T_1 and T_2 .

Under these suppositions, the Navier-Stokes's equations are [35]:

$$v_x + w_y = 0, \quad (1)$$

$$\rho_{hnf}(v_t + vv_x + ww_y) = \mu_{hnf} \left(1 + \frac{1}{\beta}\right) \nabla^2 v + \sigma B_0^2 v - P_x \quad (2)$$

$$\rho_{hnf}(w_t + vw_x + ww_y) = \mu_{hnf} \left(1 + \frac{1}{\beta}\right) \nabla^2 w + \sigma B_0^2 w - P_y \quad (3)$$

$$T_t + vT_x + wT_y = \alpha_{hnf} \nabla^2 T + \tau \left(D_B T_y + \frac{D_T}{T_2} T_{y^2} \right) + \frac{\mu_{hnf}}{(\rho c p)_{hnf}} (v_y)^2 \quad (4)$$

The boundary conditions for the above model are:

$$\begin{cases} v = 0, & w = -Aa'(t), \text{ at } y = -a(t), \text{ when } T = T_1, \\ v = 0, & w = Aa'(t), \text{ at } y = a(t), \text{ when } T = T_2, \end{cases} \quad (5)$$

where A is the wall permeability component and derivative for time, and T_1 and T_2 represent the temperature of the lower and upper walls of the permeable channel.

First of all, the continuity equation is satisfied by the similarity variables stated in Equation (6). Furthermore, the similarity variables are used in the governing equations to acquire Equations (7) and (8):

$$\eta = \frac{y}{a}, \quad v = \frac{-xv_f}{a^2} F_\eta(\eta, t), \quad w = \frac{v_f}{a} F(\eta, t), \quad \theta = \frac{T - T_2}{T_1 - T_2}, \quad (6)$$

$$\frac{v_{hnf}}{v_f} \left(1 + \frac{1}{\beta}\right) F_{\eta\eta\eta\eta} + \alpha(3F_{\eta\eta} + \eta F_{\eta\eta\eta}) + F_\eta F_{\eta\eta} - FF_{\eta\eta} + \frac{\rho_{bfl}}{\rho_{hnf}} MF_{\eta\eta} - \frac{a^2}{v_f} F_{\eta\eta t} = 0 \quad (7)$$

$$\frac{\alpha_{hnf}}{v_f} \theta_{\eta\eta} + \theta_\eta(\eta\alpha - F) + Nb \theta_\eta + Nt \theta_\eta^2 + \left(\frac{\mu_{hnf}}{\mu_{bfl}}\right) \left(\frac{(\rho c p)_{bfl}}{(\rho c p)_{hfl}}\right) Ec F_{\eta\eta}^2 + \frac{a^2}{v_f} \theta_t = 0 \quad (8)$$

Here, $Nt = \frac{\tau D_T \Delta T}{T_2 v_f}$, $Nb = \frac{\tau D_T \Delta C}{v_f}$, $Ec = \frac{v^2 x^2}{a^2 \Delta T (C_P)_{bfl}}$, with boundary conditions

$$\begin{cases} F = -Re, & F_\eta = 0, & \theta = -1, \text{ at } \eta = -1 \\ F = Re, & F_\eta = 0, & \theta = 1, \text{ at } \eta = 1 \end{cases} \quad (9)$$

Following Majdalani et al. [1], we assumed that t is constant, $\theta_t = F_{\eta\eta t} = 0$, and F and θ depend on η . Therefore, Equations (7) and (8) reduce to

$$\frac{v_{hnf}}{v_f} \left(1 + \frac{1}{\beta}\right) F_{\eta\eta\eta\eta} + \alpha(3F_{\eta\eta} + \eta F_{\eta\eta\eta}) + F_\eta F_{\eta\eta} - FF_{\eta\eta} + \frac{\rho_{bfl}}{\rho_{hnf}} MF_{\eta\eta} = 0 \quad (10)$$

$$\frac{\alpha_{hnf}}{v_f} \theta_{\eta\eta} + \theta_\eta(\eta\alpha - F) + Nb \theta_\eta + Nt \theta_\eta^2 + \left(\frac{\mu_{hnf}}{\mu_{bfl}}\right) \left(\frac{(\rho c p)_{bfl}}{(\rho c p)_{hfl}}\right) Ec F_{\eta\eta}^2 = 0 \quad (11)$$

Then, adjusting $f = \frac{F}{Re}$,

$$\frac{v_{hnf}}{v_f} \left(1 + \frac{1}{\beta}\right) f_{\eta\eta\eta\eta} + \alpha(3f_{\eta\eta} + \eta f_{\eta\eta\eta}) + Re(f_\eta f_{\eta\eta} - ff_{\eta\eta}) + \frac{\rho_{bfl}}{\rho_{hnf}} Mf_{\eta\eta} = 0 \quad (12)$$

$$\frac{\alpha_{hnf}}{v_f} \theta_{\eta\eta} + \theta_{\eta}(\eta\alpha - fRe) + Nb \theta_{\eta} + Nt \theta_{\eta}^2 + \left(\frac{\mu_{hnf}}{\mu_{bfl}} \right) \left(\frac{(\rho c_p)_{bfl}}{(\rho c_p)_{hnf}} \right) Ec(Re)^2 f_{\eta\eta}^2 = 0 \quad (13)$$

Here, $v_{hnf} = \frac{\mu_{hnf}}{\rho_{hnf}}$, $\alpha_{hnf} = \frac{k_{hnf}}{(\rho c_p)_{hnf}}$. ρ_{hnf} represents the density of (HNfl), P is the pressure, v_{hnf} is the kinematic viscosity of (HNfl), σ is the electrical conductivity, B_0 is the strength of the magnetic field, α_{hnf} is the thermal diffusivity, and T is the temperature.

The thermophysical properties of nanoparticles and base fluid are given in Table 1, while the properties of HNfl are given in Table 2.

Table 1. Description of the thermophysical properties of nanoparticles and base fluid [24].

Nanoparticles and Base Fluid	Molecular Formula	Density, ρ (kg/m ³)	Specific Heat, C_p (J/kg·K)	Thermal Conductivity, k (W/m·k)
Titanium dioxide (titania)	TiO ₂	4250	686.2	8.954
Silver	Ag	10,500	235	429
Blood	-	1063	3594	0.492

Table 2. Thermophysical properties of HNfl [38,39].

Hybrid Nanofluids	
Density	$\rho_{hnf} = \varphi_1 \rho_1 + \varphi_2 \rho_2 + (1 - \varphi_1 - \varphi_2) \rho_{bf}$
Viscosity	$\mu_{hnf} = \mu_{bf} (1 - \varphi_1 - \varphi_2)^{-2.5}$
Heat capacity	$(\rho c_p)_{hnf} = \varphi_1 (\rho c_p)_1 + \varphi_2 (\rho c_p)_2 + (1 - \varphi_1 - \varphi_2) (\rho c_p)_{bf}$
Thermal conductivity of Nano-layer	$\frac{k_{hnf}}{k_{bf}} = \frac{(k_2 - k_{nlr}) \varphi_2 k_{nlr} (\lambda_2^2 - \lambda_1^2 + 1) + (k_2 + k_{nlr}) \lambda_2^2 (\varphi_2 \lambda_1^2 (k_{nlr} - k_{bf}) + k_{bf})}{\lambda_2^2 (k_2 + k_{nlr}) - (k_2 - k_{nlr}) \varphi_2 (\lambda_2^2 + \lambda_1^2 - 1)}$
	$\frac{k_{nf}}{k_{bf}} = \frac{(k_1 - k_{nlr}) \varphi_1 k_{nlr} (\lambda_2^2 - \lambda_1^2 + 1) + (k_1 + k_{nlr}) \lambda_2^2 (\varphi_1 \lambda_1^2 (k_{nlr} - k_{bf}) + k_{bf})}{\lambda_2^2 (k_1 + k_{nlr}) - (k_1 - k_{nlr}) \varphi_1 (\lambda_2^2 + \lambda_1^2 - 1)}$

Because those traditional models are insufficient to capture the abnormally increased thermal conductivity of the nanofluid, we did not use the classical thermal conductivity correlations outlined by renowned Maxwell [40] and Hamilton and Crosser [41]. This fundamental flaw stems from the fact that the thermal conductivity correlations in those classical models do not take into account the presence of molecular solid-liquid interfaces or nanoparticle diameter. Here, φ_1 and φ_2 represent the volume fraction of titania and silver nanoparticles. ρ_{bf} , ρ_1 , and ρ_2 represent the density of the base fluid, the first nanoparticle, and the second nanoparticle, respectively. μ_{hnf} represents the viscosity of HNfl, μ_{bf} represents the viscosity of the base fluid, $(\rho c_p)_1$ and $(\rho c_p)_2$ represent the heat capacitance for solid nanoparticles, and $(\rho c_p)_{bf}$ represents the heat capacitance for base fluid. $\lambda_1 = 1 + \frac{h}{r}$, $\lambda_2 = 1 + \frac{h}{2r}$, and in this model, h denotes the thickness of the nanolayer at the nanoparticles liquid interface, r is the radius of the particles, $k_{nlr} = 3k_{bf}$ is the thermal conductivity of the nanolayer reference [42], k_{hnf} is the thermal conductivity of the HNfl, k_{nf} is the thermal conductivity of the Nfl, and k_1 and k_2 are the thermal conductivity of hybrid nano-particles, respectively.

By replacing the formulas from Table 2, the equation becomes

$$\left(\frac{1}{(1 - \varphi_1 - \varphi_2)^{2.5} \left((1 - \varphi_1 - \varphi_2) + (\varphi_1) \left(\frac{\rho_1}{\rho_{bf}} \right) + (\varphi_2) \left(\frac{\rho_2}{\rho_{bf}} \right) \right)} \right) \left(1 + \frac{1}{\beta} \right) f'''' + \alpha (3f'' + \eta f''') + Re(f' f'' - f f''') + \left(\frac{1}{\left((1 - \varphi_1 - \varphi_2) + (\varphi_1) \left(\frac{\rho_1}{\rho_{bf}} \right) + (\varphi_2) \left(\frac{\rho_2}{\rho_{bf}} \right) \right)} \right) M f'' = 0 \quad (14)$$

$$\begin{aligned}
& \left(\frac{(k_2 - k_{nlr})\varphi_2 k_{nlr}(\lambda_2^2 - \lambda_1^2 + 1) + (k_2 + k_{nlr})\lambda_2^2(\varphi_2 \lambda_1^2(k_{nlr} - k_{bf}) + k_{bf})}{\lambda_2^2(k_2 + k_{nlr}) - (k_2 - k_{nlr})\varphi_2(\lambda_2^2 + \lambda_1^2 - 1)} \right) \\
& \left(\frac{(k_1 - k_{nlr})\varphi_1 k_{nlr}(\lambda_2^2 - \lambda_1^2 + 1) + (k_1 + k_{nlr})\lambda_2^2(\varphi_1 \lambda_1^2(k_{nlr} - k_{bf}) + k_{bf})}{\lambda_2^2(k_1 + k_{nlr}) - (k_1 - k_{nlr})\varphi_1(\lambda_2^2 + \lambda_1^2 - 1)} \right) \theta'' + \\
& Pr \left((1 - \varphi_1 - \varphi_2) + (\varphi_1) \left(\frac{(\rho c_p)_1}{(\rho c_p)_{bf}} \right) + (\varphi_2) \left(\frac{(\rho c_p)_2}{(\rho c_p)_{bf}} \right) \right) (\theta'(\eta\alpha - fRe) + Nb\theta' + Nt(\theta')^2) + \\
& (1 - \varphi_1 - \varphi_2)^{-2.5} Pr Ec(Re) 2(f'')^2 = 0
\end{aligned} \quad (15)$$

with the boundary conditions

$$\begin{cases} f = -1, & f' = 0, & \theta = 1, & \text{at } \eta = -1 \\ f = 1, & f' = 0, & \theta = 1, & \text{at } \eta = 1, \end{cases} \quad (16)$$

Here, $\alpha = \frac{a(t)a'(t)}{v_f}$ is a time-dependent dimensionless parameter and shows the expansion and contraction of the channel's walls. It is positive in the case of expansion and negative in the case of contraction. An important parameter that shows the injection and suction of the walls of the channel is the Reynold number $Re = \frac{A\alpha a'}{v_f}$; for injection case, $Re > 0$, and in suction case, $Re < 0$.

2.1. Numerical Procedure

We used Mathematica's built-in function and solved a system of nonlinear Equations (14) and (15) by using boundary conditions numerically. We utilized the software Mathematica since it has thousands of built-in functions that allow us to perform sophisticated analyses in a short amount of time. The numerical solution was obtained rather than using analytical methods. The shooting technique was used in conjunction with the fourth-order RK method for numerical computations. The Runge-Kutta method is a preferable alternative since it requires less computing, is more stable, and produces accurate results in less time. The rapidity (computational cost) and additivity of this technique to IVP are its main advantages. Finding the IVP (initial value problem) using an appropriate shooting approach is massively successful because of the importance of IVP in real-world/practical applications,

$$G_1 = \left(\frac{1}{(1 - \varphi_1 - \varphi_2)^{2.5} \left((1 - \varphi_1 - \varphi_2) + (\varphi_1) \left(\frac{\rho_1}{\rho_{bf}} \right) + (\varphi_2) \left(\frac{\rho_2}{\rho_{bf}} \right) \right)} \right) \quad (17)$$

$$G_2 = \left(\frac{1}{\left((1 - \varphi_1 - \varphi_1) + (\varphi_1) \left(\frac{\rho_1}{\rho_{bf}} \right) + (\varphi_2) \left(\frac{\rho_2}{\rho_{bf}} \right) \right)} \right) \quad (18)$$

$$G_3 = \left((1 - \varphi_1 - \varphi_2) + (\varphi_1) \left(\frac{(\rho c_p)_1}{(\rho c_p)_{bf}} \right) + (\varphi_2) \left(\frac{(\rho c_p)_2}{(\rho c_p)_{bf}} \right) \right) \quad (19)$$

$$G_4 = (1 - \varphi_1 - \varphi_2)^{-2.5} \quad (20)$$

$$Z_1 = \left(\frac{(k_2 - k_{nlr})\varphi_2 k_{nlr}(\lambda_2^2 - \lambda_1^2 + 1) + (k_2 + k_{nlr})\lambda_2^2(\varphi_2 \lambda_1^2(k_{nlr} - k_{bf}) + k_{bf})}{\lambda_2^2(k_2 + k_{nlr}) - (k_2 - k_{nlr})\varphi_2(\lambda_2^2 + \lambda_1^2 - 1)} \right) \quad (21)$$

$$Z_2 = \left(\frac{(k_1 - k_{nlr})\varphi_1 k_{nlr}(\lambda_2^2 - \lambda_1^2 + 1) + (k_1 + k_{nlr})\lambda_2^2(\varphi_1 \lambda_1^2(k_{nlr} - k_{bf}) + k_{bf})}{\lambda_2^2(k_1 + k_{nlr}) - (k_1 - k_{nlr})\varphi_1(\lambda_2^2 + \lambda_1^2 - 1)} \right) \quad (22)$$

By inputting the values of G_1 , G_2 , G_3 , G_4 , Z_1 , and Z_2 the equations become:

$$G_1 \left(1 + \frac{1}{\beta} \right) f''' + \alpha (3f'' + \eta f''') + Re(f' f'' - f f''') + G_2 M f'' = 0 \quad (23)$$

$$Z_1 Z_2 \theta'' + Pr G_3 (\theta' (\eta \alpha - f Re) + Nb \theta' + Nt (\theta')^2) + G_4 Br (Re)^2 (f'')^2 = 0 \quad (24)$$

As we proceed, the ruling set of PDEs was transformed into the following system of first-order ODEs; let $f' = m$, $f'' = n$, $f''' = p$, and $\theta' = q$, and by substituting values in Equations (23) and (24), the equations become:

$$p' = - \left(\frac{1}{G_1} \right) \left(\frac{\beta}{1 + \beta} \right) [\alpha (3n + \eta p) + Re(mn - fp) + G_2 Mn] \quad (25)$$

$$q' = - \frac{1}{Z_1 Z_2} q [Pr G_3 ((\eta \alpha - f Re) + Nt q) + G_4 Br (Re)^2 (m)^2] \quad (26)$$

Associated boundary conditions,

$$\begin{aligned} f(-1) &= -1, & m(-1) &= -1, & \theta(-1) &= 1, & n(-1) &= a_1, \\ p(-1) &= a_2, & q(-1) &= a_3. \end{aligned}$$

Here, a_1 , a_2 , and a_3 are the initial missing conditions.

2.2. Engineering Interest Quantities

2.2.1. Skin Friction Coefficients

C_{f1} and the C_{f-1} represent the coefficient of skin friction of the upper and lower porous channel walls that is expressed as:

$$\begin{aligned} C_{f1} &= \frac{\zeta_y|_{\eta=1}}{\rho_{f(a'A)}^2} = \frac{1}{Re_r(1 - \varphi_1 - \varphi_2)^{2.5}} f''(1) \\ C_{f-1} &= \frac{\zeta_y|_{\eta=-1}}{\rho_{f(a'A)}^2} = \frac{1}{Re_r(1 - \varphi_1 - \varphi_2)^{2.5}} f''(-1) \end{aligned}$$

ζ_y are shear stresses at the lower and upper porous channel walls in the radial direction, respectively,

$$\begin{aligned} \zeta_y &= \mu_{hnf}(v_y)|_{\eta=1} = \frac{\mu_{bf}}{(1 - \varphi_1 - \varphi_2)^{2.5}} \left(\frac{rv_f}{a^3} \right) f''(1) \\ \zeta_y &= \mu_{hnf}(v_y)|_{\eta=-1} = \frac{\mu_{bf}}{(1 - \varphi_1 - \varphi_2)^{2.5}} \left(\frac{rv_f}{a^3} \right) f''(-1) \end{aligned}$$

2.2.2. Nusselt Numbers

The calculation at the lower and upper porous channel walls for heat transfer rate, (Nusselt numbers) Nu_{y-1} and Nu_{y1} , are given as:

$$\begin{aligned} Nu_{y1} &= \frac{ad_y}{k_f(T_1 - T_2)}|_{\eta=1} = - \frac{k_{hnf}}{k_f} \theta'(1) \\ Nu_{y-1} &= \frac{ad_y}{k_f(T_1 - T_2)}|_{\eta=-1} = - \frac{k_{hnf}}{k_f} \theta'(-1) \end{aligned}$$

Here, heat flux is denoted as d_y , which follows as:

$$\begin{aligned} d_y|_{\eta=1} &= -k_{hnf}(T_y)|_{\eta=1} = - \frac{(T_1 - T_2)}{a} k_{hnf} \theta'(1) \\ d_y|_{\eta=-1} &= -k_{hnf}(T_y)|_{\eta=-1} = - \frac{(T_1 - T_2)}{a} k_{hnf} \theta'(-1) \end{aligned}$$

where

$$Re = \frac{Aaa'(t)}{v_f}$$

3. Result and Discussion

The nonlinear differential equations were solved numerically by the shooting method with the respective boundary conditions. Additionally, the physical behavior of the parameters involved in the velocity, temperature, and concentration distribution was examined. We assigned the values for the flowing parameters such as M , β , Re , Br , Pr , Nt , Nb , h , r , α , φ_1 , and φ_2 elsewhere. All of these values are kept constant, except the variable one, for each computation, which is significant in graphs and tables. The velocity, temperature, and concentration distribution graphs are represented in the whole discussion by the hybrid nanofluid case. Table 1 illustrates the thermo-physical properties of titanium dioxide, silver, and blood. In Table 2 the thermophysical properties of hybrid nanofluids are represented. Table 3 represents the effect of the nano-layer thickness (h), the radius of the nanoparticle (r), and the volume of fraction (φ_1 , φ_2) on thermal conductivity. As we increased the value of φ_1 , φ_2 , and h , the thermal conductivity of the hybrid nanofluid increased, but in the case of increasing r , the value of thermal conductivity decreased. Tables 4 and 5 show the comparison of nano and hybrid nanofluid in different non-dimensionless parameters with the impact of the skin friction coefficient and Nusselt number. The results of the skin friction coefficient show better results on nanofluid with (TiO_2 /Blood) by increasing the volume fraction, but the numerical results of the Nusselt number gave efficient readings in hybrid nanofluid ($TiO_2 - Ag$ /Blood) in both upper and lower porous walls. Furthermore, with $Re < 0$ and $\alpha > 0$, the skin friction coefficient and Nusselt numbers showed gradually reducing behavior in both porous cases, except the effect of the Reynolds number on the Nusselt number showed increasing behavior in both upper and lower walls. Table 6 illustrates the impact of heat transfer rate on thermophoresis and Brownian motion. If we enhanced the values of Nt and Nb , the heat transfer rate increased on the upper wall and decreased on the lower wall of the channel. Table 7 shows the analyses of heat transfer rate on several parameters such as the Prandtl number, Brickman number, nano-layer thickness, and radius of the particle. If we rose the values of Br and h , then the flow of heat transfer rate in hybrid nanofluids ($TiO_2 - Ag$ /Blood) escalated. Furthermore, with $r > 0$ for the flow of nanoparticles, the heat transfer rate was minimized, while on the other hand, the opposite numerical results of heat transfer were concluded on both walls of the channel by the raising Prandtl number. Physically, the Prandtl number is the ratio of thermal diffusivity and momentum diffusivity. Table 8 shows the numerical comparison of the previous result and the current study flow of momentum and thermal transfer on a lower surface. Figure 1 shows an interesting behavior of shear stress and Casson fluid parameter (β). Increasing the values of the Casson fluid parameter caused the shear stress on fluid to gradually increase, and the fluid showed Newtonian behavior on the infinite values, showed Non-Newtonian behavior on small values, and behaved like a solid on zero values of the Casson fluid parameter (β). Figure 2 displays the diagram of the problem. Figure 3 expresses variation in the thermal conductivity of the hybrid nanofluid against (h) and (r) on five different numerical values of volume fraction. We observed that, by increasing (h), thermal conductivity gradually increased and gradually decreased by increasing (r). Figure 4 shows the comparison results of nano and hybrid nanofluids, while the hybrid nanofluids showed excellent results. Figure 5 demonstrates the effect of expanding the contracting parameter α on the velocity profile. If α varied from negative to positive, then the momentum boundary layer thickness increased at the center of the wall and decreased on both upper and lower porous walls. Figure 6 describes the increasing behavior of the temperature profile on both lower and upper walls through the impact of expanding the contracting parameter α . Figures 7 and 8 clarify the effect of the Reynolds number and magnetic parameter of the velocity profile by taking Re and M in increasing order. Increasing the value of the Reynolds number and the magnetic parameter, the momentum boundary layer thickness increased at the center of the wall and showed decreasing behavior on both upper and lower walls. In Figure 9, it is observed that, by increasing the value of the permeable Reynolds number, there were high values of temperature profile on both of the walls and at the center of the wall. Figure 10 shows that, if we took high values of the Casson fluid parameter, then the velocity profile increased in the middle of the wall and decreased on upper and lower porous walls.

Table 3. Effect of nano-layer thickness (h), radius (r), and volume fraction (φ_1, φ_2) of particles on T.C (K_{hmf}) for $Pr = 0.1$, $Br = 0.1$, $\alpha = 1$, $\beta = 0.1$, $Re = -0.5$, $Nt = Nb = 0.5$, $M = 9$.

h	r	$\varphi_1 = \varphi_2$	k_{hmf}
2	1.8	0.01 = 1%	0.1164
4			0.1750
6			0.2419
8			0.3035
10			0.3540
2	1.9	0.01 = 1%	0.1139
	2.0		0.1118
	2.1		0.1099
	2.2		0.1082
	1.8	0.02 = 2%	0.1626
		0.03 = 3%	0.2019
		0.04 = 4%	0.2354
		0.05 = 5%	0.2640

Table 4. Skin fraction and Nusselt number results on volume fraction, Reynolds number, and expansion-contraction ratio parameter for $Pr = 0.1$, $M = 9$, $Nt = Nb = 0.5$, $Br = 0.1$, $\beta = 0.1$, $h = 2$, $r = 1.5$ on different types of nanofluids.

			(TiO ₂ /Blood)				(Ag/Blood)				
φ	Re	α	$ C_{f-1} $	$ C_{f1} $	$ Nu_{y-1} $	$ Nu_{y1} $	$ C_{f-1} $	$ C_{f1} $	$ Nu_{y-1} $	$ Nu_{y1} $	
0.01 = 1%	−0.5	1	2.7602	2.7602	0.0942	0.7524	2.7556	2.7556	0.0953	0.7518	
0.02 = 2%			2.7641	2.7641	0.1228	0.7360	2.7557	2.7557	0.1252	0.7347	
0.03 = 3%			2.7681	2.7681	0.1479	0.7218	2.7558	2.7558	0.1518	0.7196	
0.04 = 4%			2.7721	2.7721	0.1701	0.7093	2.7561	2.7561	0.1755	0.7061	
0.01 = 1%			2.7580	2.7580	0.6305	1.4659	2.7536	2.7536	0.6278	1.4637	
	−1	2	2.7558	2.7558	1.7770	2.6307	2.7513	2.7513	1.7710	2.6258	
	−1.5		2.7536	2.7536	3.3371	4.2354	2.7490	2.7490	3.3286	4.2269	
	−2.0		2.6870	2.6870	0.0706	0.6739	2.6785	2.6785	0.0718	0.6737	
	−0.5		3	2.6141	2.6141	0.0501	0.6028	2.6016	2.6016	0.0513	0.6027
			4	2.5417	2.5417	0.0325	0.5385	2.5252	2.5252	0.0337	0.5385

Table 5. Skin fraction and Nusselt number results on volume fraction, Reynolds number, and expansion-contraction ratio parameter for $Pr = 0.1$, $M = 9$, $Nt = Nb = 0.5$, $Br = 0.1$, $\beta = 0.1$, $h = 2$, $r = 1.5$ on hybrid nanofluids.

				(TiO ₂ –Ag/Blood)			
φ_1	φ_2	Re	α	$ C_{f-1} $	$ C_{f1} $	$ Nu_{y-1} $	$ Nu_{y1} $
0.01 = 1%	0.01 = 1%	−0.5	1	2.7599	2.7599	0.1262	0.7339
0.02 = 2%				2.7640	2.7640	0.1530	0.7185
0.03 = 3%				2.7681	2.7681	0.1764	0.7052
0.04 = 4%				2.7721	2.7721	0.1971	0.6936
0.01 = 1%				2.7599	2.7599	0.1543	0.7178
	0.02 = 2%	−1	2	2.7601	2.7601	0.1791	0.7036
	0.03 = 3%			2.7605	2.7605	0.20131	0.6911
	0.04 = 5%			2.7576	2.7576	0.5512	1.3975
	0.01 = 1%	−1.5		2.7553	2.7553	1.6254	2.4829
		−2.0		2.7530	2.7530	3.0869	3.9777
		−0.5	2	2.6825	2.6825	0.1026	0.6650
				2.6055	2.6055	0.0817	0.6017
				2.5290	2.5290	0.0633	0.5438

Table 6. Heat transfer result on thermophoresis motion and Brownian motion for $Pr = 0.1$, $M = 9$, $Br = 0.05$, $\varphi_1 = \varphi_2 = 0.01$, $\alpha = 1$, $\beta = 0.1$, $h = 2$, $r = 1.5$, $Re = -0.5$ on hybrid nanofluids.

(TiO ₂ –Ag/Blood)			
Nt	Nb	$ \theta'(-1) $	$ \theta'(1) $
0.1	0.5	0.2631	0.5799
0.6		0.2345	0.6208
1.2		0.2029	0.6737
1.8		0.1741	0.7311
2.4		0.1479	0.7929
	0.8	0.2449	0.6029
	1.1	0.2274	0.6266
	1.4	0.2106	0.6509
	1.7	0.1944	0.6757

Table 7. Heat transfer result on the Prandtl number, Brickman number, Nano-layer thickness, and the radius of particle for $M = 9$, $\varphi_1 = \varphi_2 = 0.01$, $\alpha = 1$, $\beta = 0.1$, $Re = -0.5$, $Nt = Nb = 0.5$ on hybrid nanofluids.

(TiO ₂ –Ag/Blood)					
Pr	Br	h	r	$ \theta'(-1) $	$ \theta'(1) $
0.5	0.05	2	1.5	0.0091	0.5070
0.6				0.0100	0.4774
0.7				0.0220	0.4480
0.8				0.0292	0.4192
0.5				0.0620	0.6008
	0.10	4	1.6	0.1336	0.6950
	0.15			0.2054	0.7897
	0.20			0.0617	0.5172
	0.05	6		0.1367	0.5222
		8		0.2179	0.5286
			1.7	0.0068	0.5063
			1.7	0.0049	0.5057
			1.8	0.0032	0.5052

Table 8. Comparison results in momentum and heat transfer at the lower plate for $\alpha = -1$, $\varphi_1 = 0.06$, $\varphi_2 = 0.06$, $M = 1$.

Qureshi et al. [30]			Present Results	
Re	$f''(-1)$	$\theta(-1)$	$f''(-1)$	$\theta(-1)$
−1	4.19168	−0.36988	4.19169	−0.36989
−0.5	4.40338	−0.968884	4.40339	−0.968885
0	4.64876	−1.98464	4.64878	−1.98465
0.5	4.93215	−3.26874	4.93216	−3.26875
1	5.25781	−4.63023	5.25782	−4.63024

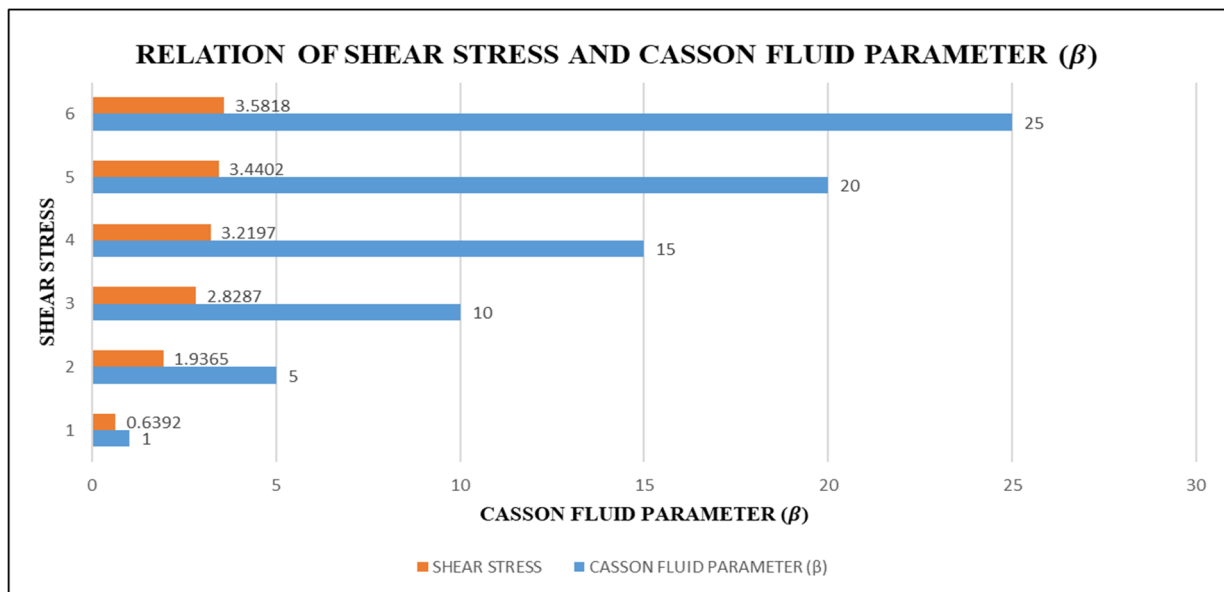


Figure 1. Variation in the behavior of fluid (Newtonian/Non-Newtonian) due to applied shear stress.

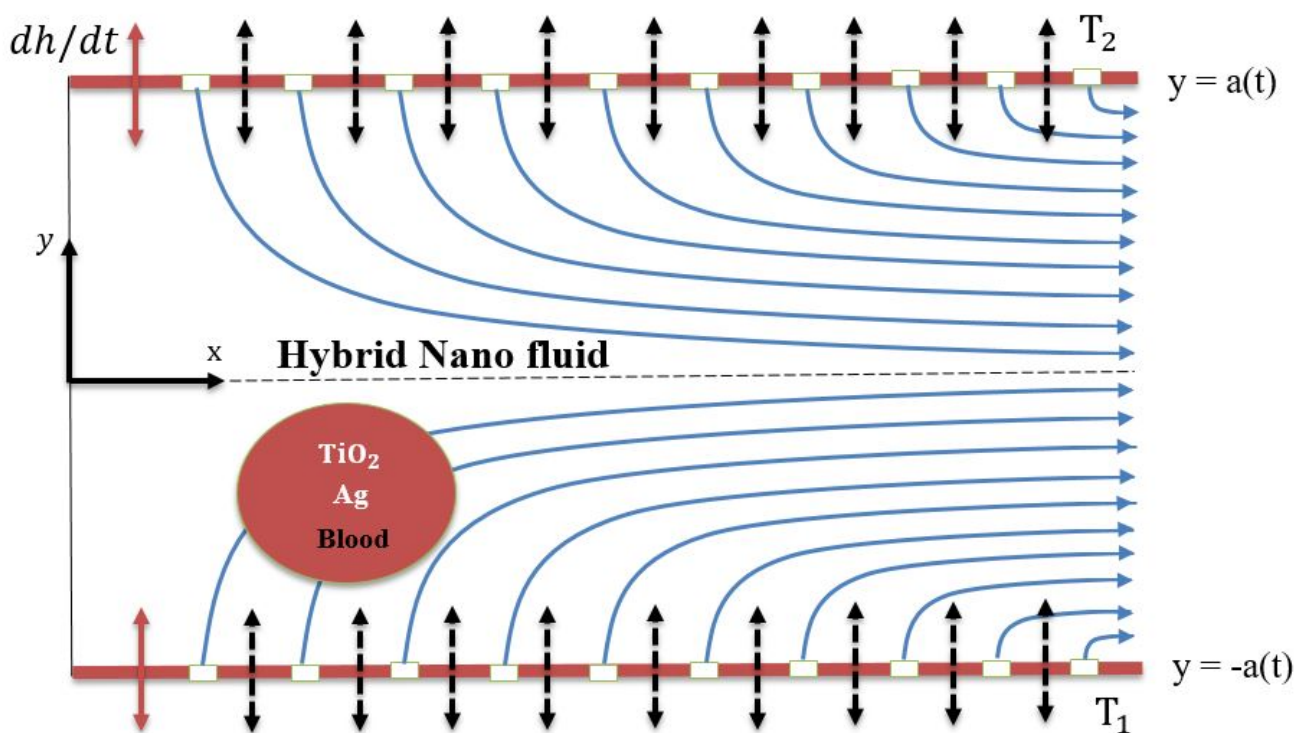
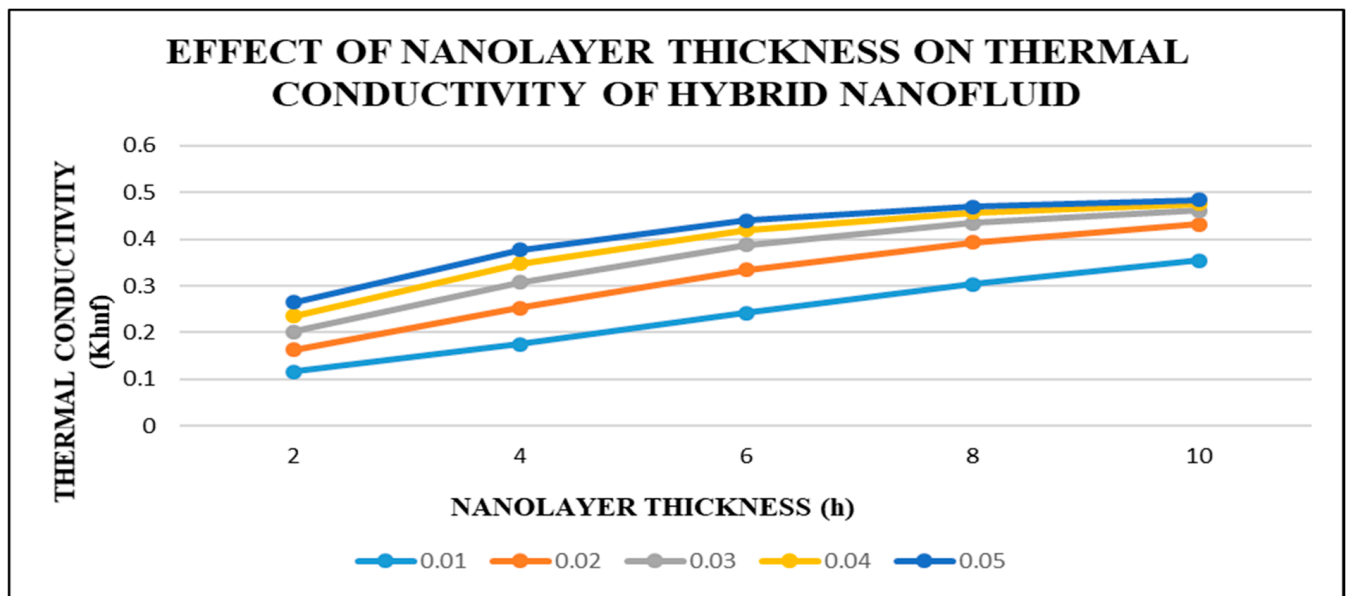
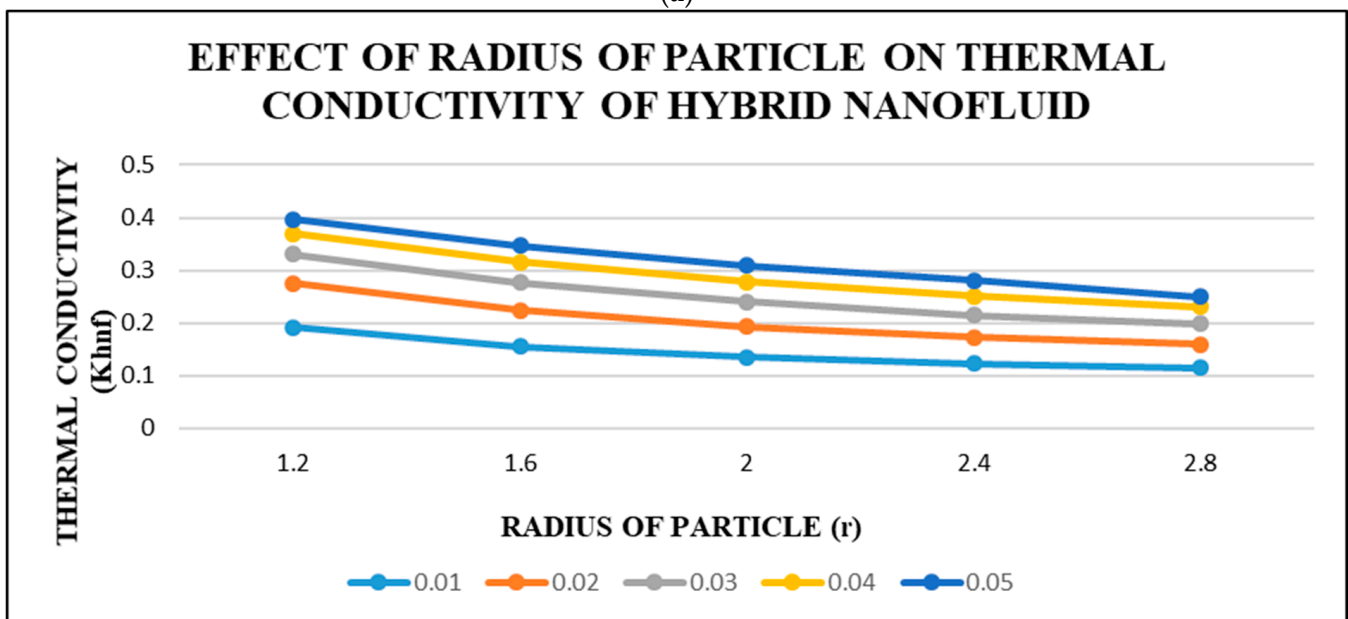


Figure 2. The schematic diagram of the problem.



(a)



(b)

Figure 3. Results of T.C. on thickness (a) and radius (b).

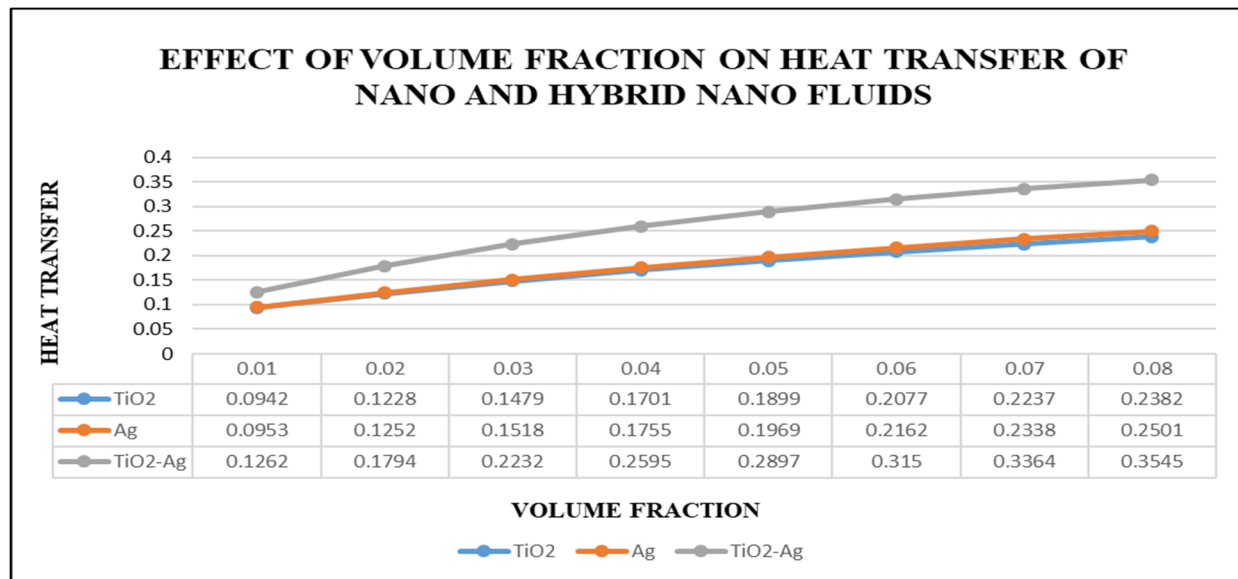


Figure 4. Influence of the volume fraction on the heat transfer rate of nano and hybrid nanofluids.

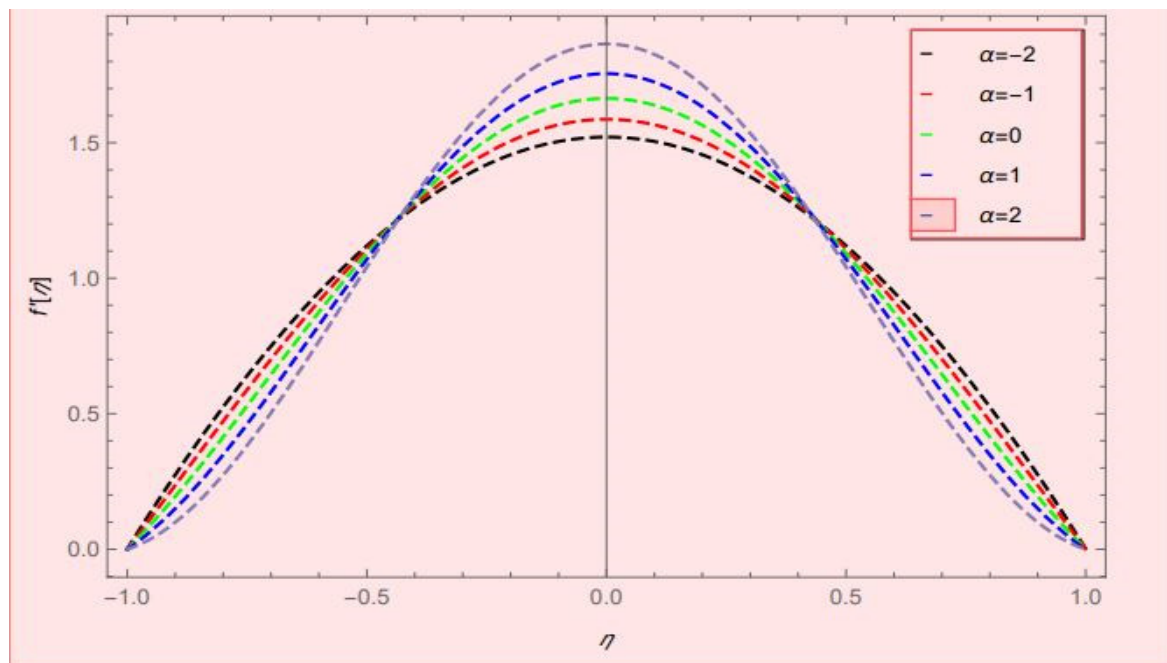


Figure 5. Velocity profile effect against the wall expansion and contraction ratio (α) for $Re = 4$, $Pr = 0.1$, $Nt = Nb = 0.7$, $M = 13$, $\beta = 0.6$, $Br = 0.1$, $\varphi_1 = \varphi_2 = 0.02$, $h = 2$, $r = 1.5$.

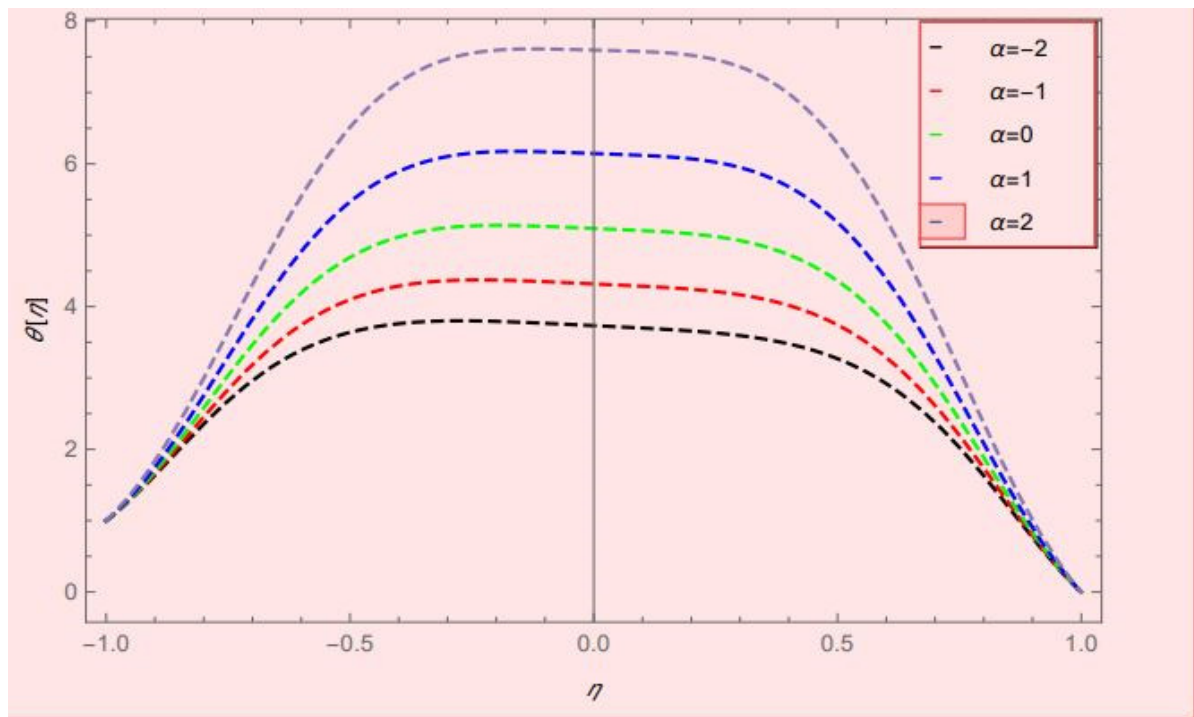


Figure 6. Temperature profile effect against the wall expansion and contraction ratio (α) for $Re = 4$, $Pr = 0.1$, $Nt = Nb = 0.7$, $M = 13$, $\beta = 0.6$, $Br = 0.1$, $\varphi_1 = \varphi_2 = 0.02$, $h = 2$, $r = 1.5$.

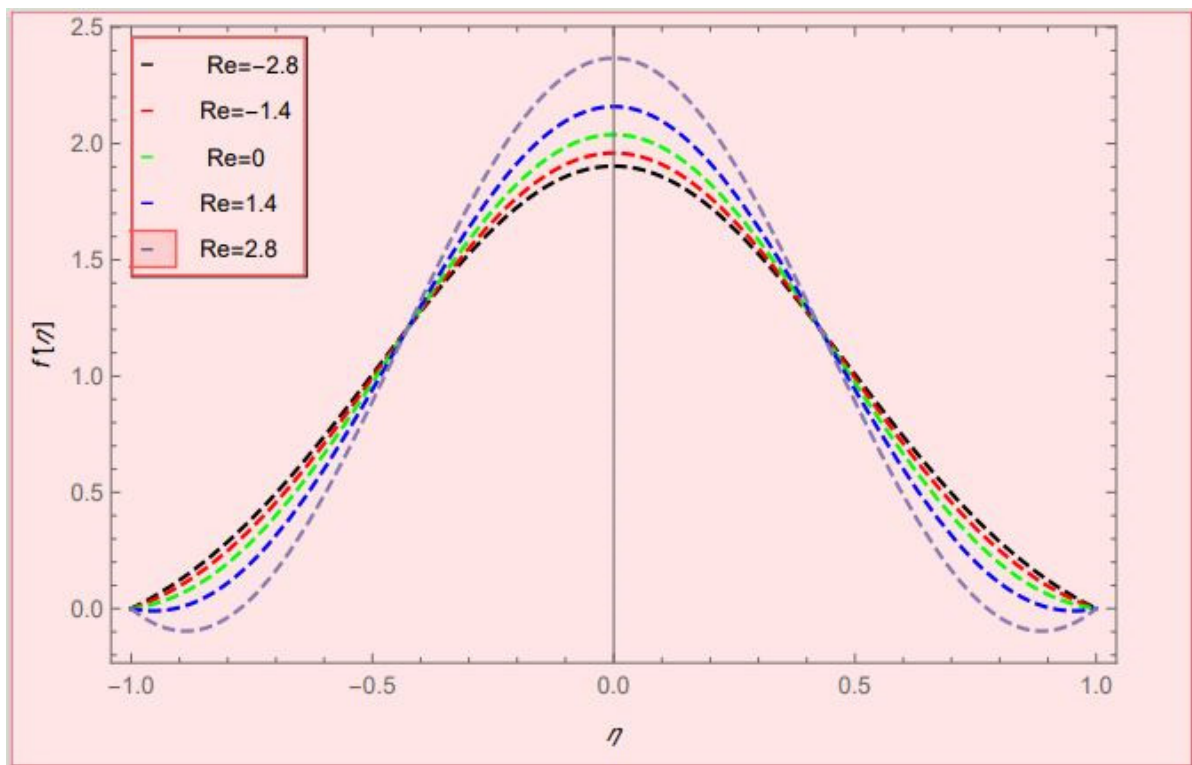


Figure 7. Velocity profile effect against the Reynolds number for $\alpha = 3.2$, $Pr = 0.1$, $Nt = Nb = 0.5$, $M = 8$, $\beta = 1.4$, $Br = 0.1$, $\varphi_1 = \varphi_2 = 0.02$, $h = 2$, $r = 1.5$.

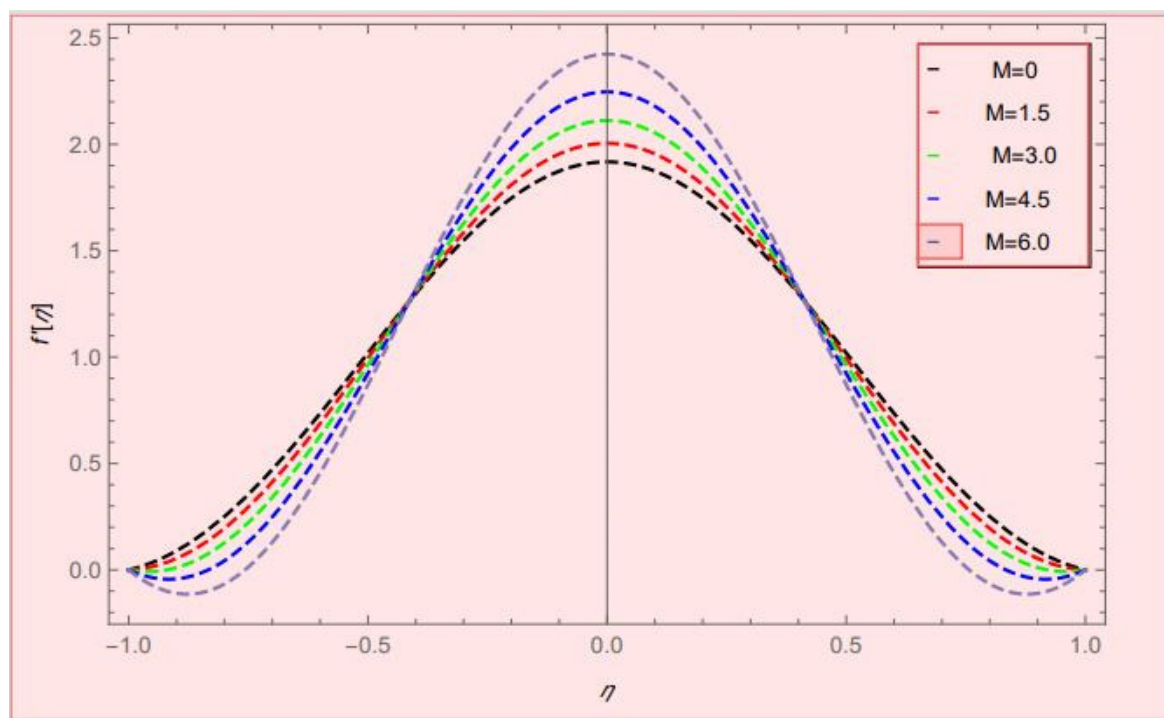


Figure 8. Velocity profile effect against the magnetic parameter (M) for $\alpha = 3.2$, $Pr = 0.1$, $Nt = Nb = 0.7$, $Re = 2.5$, $\beta = 2$, $Br = 0.1$, $\varphi_1 = \varphi_2 = 0.02$, $h = 2$, $r = 1.5$.

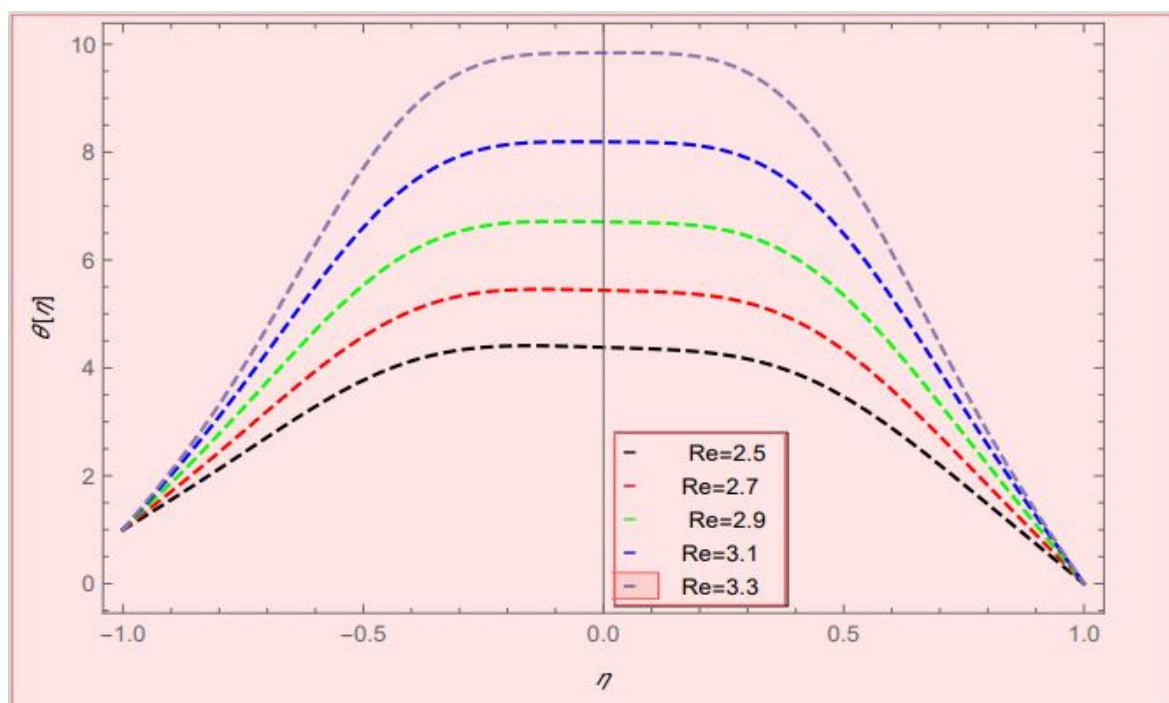


Figure 9. Temperature profile effect against the Reynolds number for $\alpha = 4$, $Pr = 0.1$, $Nt = 0.7$, $Nb = 0.7$, $M = 9$, $\beta = 1.3$, $Br = 0.03$, $\varphi_1 = \varphi_2 = 0.02$, $h = 2$, $r = 1.5$.

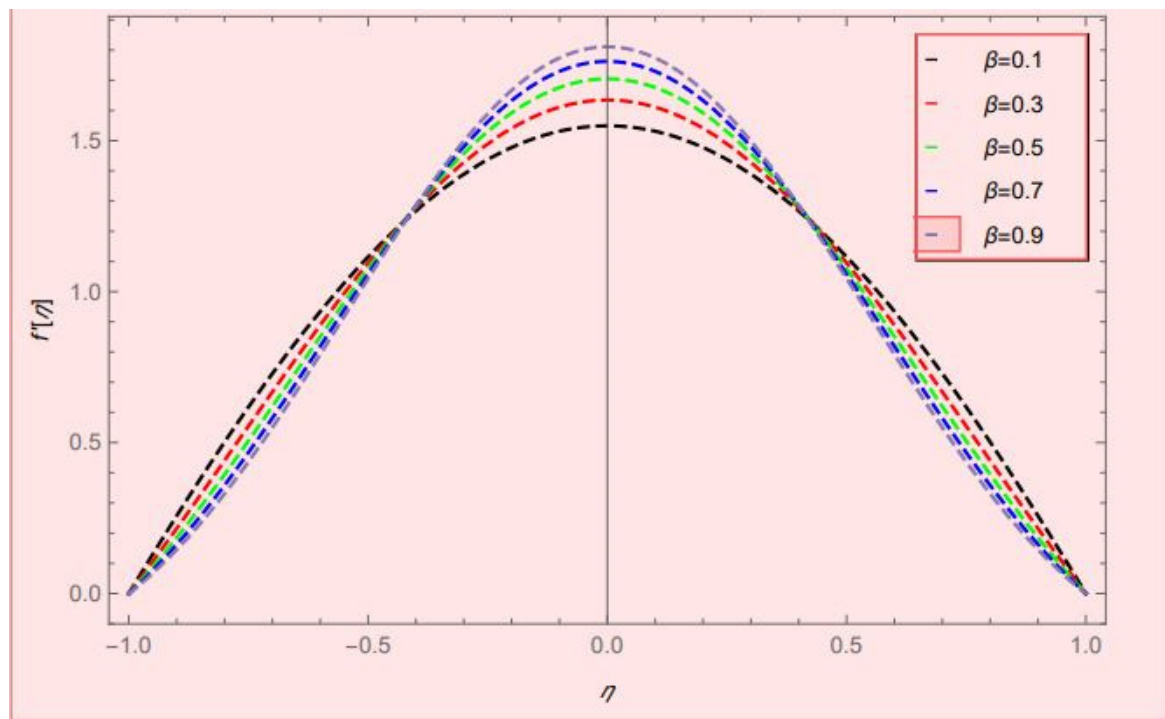


Figure 10. Velocity profile effect against the Casson fluid parameter (β) for $\alpha = 2$, $Pr = 0.1$, $Nt = Nb = 0.7$, $Re = -2.5$, $M = 12$, $Br = 0.1$, $\varphi_1 = \varphi_2 = 0.02$, $h = 2$, $r = 1.5$.

4. Conclusions/Final Result

In this article, the laminar, isothermal, unsteady, and incompressible non-Newtonian Casson hybrid nano blood flow combined with the effect of the nano-layer through a deformable porous channel in the rectangular domain was observed by using Mathematica with the help of a shooting method based on the fourth-order Runge-Kutta method. We drew the following results from this research:

- By increasing the values of φ_1 and φ_2 , the comparison of nanofluid and hybrid nanofluids gave much better results for hybrid nanofluids.
- Taking $\beta > 0$, the momentum profile decreased on both upper and lower walls and increased at the center of the channel.
- Taking $h > 0$ and $r > 0$, the thermal conductivity of hybrid nanofluids was vice versa.
- By enhancing the values of Nt and Nb , the flow of heat transfer rate gradually increased on the upper wall and decreased on the lower wall of the channel.

Finally, the important thing is that we can use hybrid nanoparticles rather than nano for improving thermal conductivity, heat transfer rate, and many other benefits, but in the case of biology we can use hybrid nanoparticles and the concept of nano-layer as tunable characteristics, as well as for improving thermal conductivity and heat transfer rate. Through this computational effort, we have successfully elucidated the parametric impacts on the dynamics of the Casson hybrid nanofluid. This study may be extended for tri-hybrid nanofluid and various physical properties of nanoparticles such as nanoparticle radius, shapes, inter-particle spacing, and aggregation.

Author Contributions: Software, M.M.A.; validation, A.A.H.; formal analysis, M.A.R.; investigation, M.Z.A.Q.; writing—original draft, Q.R.; writing—review and editing, N.A.S.; project administration, B.A. All authors have read and agreed to the published version of the manuscript.

Funding: The authors extend their appreciation to the Deputyship for Research and Innovation, Ministry of Education in Saudi Arabia for funding this research work through the project number RI-44-0360.

Data Availability Statement: Not applicable.

Acknowledgments: The authors extend their appreciation to the Deputyship for Research and Innovation, Ministry of Education in Saudi Arabia for funding this research work through the project number RI-44-0360.

Conflicts of Interest: The authors declare no conflict of interest.

Nomenclature

u, v	velocity components along the x and y-axis
T	temperature (K)
P	pressure (N/m ²)
B_0	magnetic strength
A	permeability component
c_p	specific heat at constant pressure
σ	electrical conductivity
ν	kinematic viscosity
β	Casson fluid parameter
α	contraction/expansion parameter
ρ	fluid density
D_B	Brownian diffusion constant (m ² /s)
D_T	thermophoresis diffusion coefficient (m ² /s)
α_{hnf}	thermal diffusivity of hybrid nanofluids
θ	temperature profile
h	momentum layer thickness
r	radius of the particle
η	boundary layer condition
φ_1, φ_2	volume fraction
Br	Brickman number
Pe	Peclet number
k_{hnf}	thermal conductivity of hybrid nanofluid
k_{bfd}	thermal conductivity of the base fluid
k_1	thermal conductivity of 1st particle
k_2	thermal conductivity of 2nd particle
ν_{hnf}	kinematic viscosity of hybrid nanofluid
ν_{bfd}	kinematic viscosity of the base fluid
ρ_{hnf}	density of hybrid nanofluid
ρ_{bfd}	density of the base fluid
μ_{hnf}	viscosity of hybrid nanofluid
μ_{bfd}	viscosity of the base fluid
$c_{p_{hnf}}$	heat capacitance of hybrid nanofluid
$c_{p_{bfd}}$	heat capacitance of base fluid
$HNfl$	hybrid nanofluid
$Pr = \left(\frac{(\mu C_p)_{bf}}{k_{bf}} \right)$	Prandtl number
$Re = \left(\frac{Aaa' / v_f}{\nu_f} \right)$	Reynolds number
$M = \left(\frac{\sigma B^2 a^2}{v_f \rho} \right)$	magnetic parameter
$Ec = \left(\frac{v^2 x^2 / a^2 \Delta T (C_p)_{bf}}{\nu_f} \right)$	Eckert number
$Nb = \left(\frac{\tau D_T \Delta C}{v_f} \right)$	Brownian motion parameter.
$Nt = \left(\frac{\tau D_T \Delta T}{v_f T_2} \right)$	thermophoresis motion parameter

References

1. Majdalani, J.; Zhou, C.; Dawson, C. Two-dimensional viscous flow between slowly expanding or contracting walls with weak permeability. *J. Biomech.* **2002**, *35*, 1399–1403. [[CrossRef](#)]
2. Umavathi, J.; Chamkha, A.; Mateen, A.; Al-Mudhaf, A. Unsteady oscillatory flow and heat transfer in a horizontal composite porous medium channel. *Nonlinear Anal. Model. Control.* **2009**, *14*, 397–415. [[CrossRef](#)]

3. Choi, S. Enhancing thermal conductivity of fluids with nanoparticles. *ASME-Publications-Fed.* **1995**, *231*, 99–106.
4. Ali, N.; Teixeira, J.; Addali, A. A Review on Nanofluids: Fabrication, Stability, and Thermophysical Properties. *J. Nanomater.* **2018**, *2018*, 1–33. [\[CrossRef\]](#)
5. Sundar, L.; Sharma, K.V.; Singh, M.; Sousa, A. Hybrid nanofluids preparation, thermal properties, heat transfer and friction factor—A review. *Renew. Sustain. Energy Rev.* **2017**, *68*, 185–198. [\[CrossRef\]](#)
6. Sarkar, J.; Ghosh, P.; Adil, A. A review on hybrid nanofluids: Recent research, development and applications. *Renew. Sustain. Energy Rev.* **2015**, *43*, 164–177. [\[CrossRef\]](#)
7. Suganthi, K.; Rajan, K. Metal oxide nanofluids: Review of formulation, thermo-physical properties, mechanisms, and heat transfer performance. *Renew. Sustain. Energy Rev.* **2017**, *76*, 226–255. [\[CrossRef\]](#)
8. Elsaid, K.; Olabi, A.; Wilberforce, T.; Abdelkareem, M.; Sayed, E. Environmental impacts of nanofluids: A review. *Sci. Total Environ.* **2020**, *763*, 144202. [\[CrossRef\]](#) [\[PubMed\]](#)
9. Wole-oshio, I.; Okonkwo, E.; Abbasoglu, S.; Kavaz, D. Nanofluids in Solar Thermal Collectors: Review and Limitations. *Int. J. Thermophys.* **2020**, *41*, 1–74. [\[CrossRef\]](#)
10. Le Ba, T.; Mahian, O.; Wongwises, S.; Szilágyi, I. Review on the recent progress in the preparation and stability of graphene-based nanofluids. *J. Therm. Anal. Calorim.* **2020**, *142*, 1145–1172. [\[CrossRef\]](#)
11. Yu, W.; Xie, H. A review on nanofluids: Preparation, stability mechanisms, and applications. *J. Nanomater.* **2011**, *2012*, 1–17. [\[CrossRef\]](#)
12. He, Y.; Jin, Y.; Chen, H.; Ding, Y.; Cang, D.; Lu, H. Heat transfer and flow behaviour of aqueous suspensions of TiO₂ nanoparticles (nanofluids) flowing upward through a vertical pipe. *Int. J. Heat Mass Transf.* **2007**, *50*, 2272–2281. [\[CrossRef\]](#)
13. Li, J. *Computational Analysis of Nanofluid Flow in Microchannels with Applications to Micro-Heat Sinks and Bio-MEMS*; NC State University: Raleigh, NC, USA, 2008.
14. Mishra, A.; Ram, S.; Ghosh, G. Dynamic Light Scattering and Optical Absorption in Biological Nanofluids of Gold Nanoparticles in Poly(vinyl pyrrolidone) Molecules. *J. Phys. Chem. C* **2009**, *113*, 6976–6982. [\[CrossRef\]](#)
15. Ebrahimi-Bajestan, E.; Moghadam, M.C.; Niazmand, H.; Daungthongsuk, W.; Wongwises, S. Experimental and numerical investigation of nanofluids heat transfer characteristics for application in solar heat exchangers. *Int. J. Heat Mass Transf.* **2016**, *92*, 1041–1052. [\[CrossRef\]](#)
16. Ali, H.; Babar, H.; Shah, T.; Sajid, M.; Qasim, M.; Javed, S. Preparation Techniques of TiO₂ Nanofluids and Challenges: A Review. *Appl. Sci.* **2018**, *8*, 587. [\[CrossRef\]](#)
17. Dakshayani, S.S.; Marulasiddeshwara, M.B.; Kumar, S.; Golla, R.; Devaraja, S.R.H.K.; Hosamani, R. Antimicrobial, anticoagulant and antiplatelet activities of green synthesized silver nanoparticles using Selaginella (Sanjeevini) plant extract. *Int. J. Biol. Macromol.* **2019**, *131*, 787–797. [\[CrossRef\]](#)
18. Brzóska, K.; Golba, A.; Kuczak, M.; Mrozek-Wilczkiewicz, A.; Boncel, S.; Dzida, M. Bio-Based Nanofluids of Extraordinary Stability and Enhanced Thermal Conductivity as Sustainable Green Heat Transfer Media. *ACS Sustain. Chem. Eng.* **2021**, *9*, 7369–7378. [\[CrossRef\]](#)
19. Jana, S.; Salehi-Khojin, A.; Zhong, W.-H. Enhancement of fluid thermal conductivity by the addition of single and hybrid nano-additives. *Thermochim. Acta* **2007**, *462*, 45–55. [\[CrossRef\]](#)
20. Jha, N.; Ramaprabhu, S. Synthesis and Thermal Conductivity of Copper Nanoparticle Decorated Multiwalled Carbon Nanotubes Based Nanofluids. *J. Phys. Chem. C* **2008**, *112*, 9315–9319. [\[CrossRef\]](#)
21. Madhesh, D.; Parameshwaran, R.; Kalaiselvam, S. Experimental investigation on convective heat transfer and rheological characteristics of Cu–TiO₂ hybrid nanofluids. *Exp. Therm. Fluid Sci.* **2014**, *52*, 104–115. [\[CrossRef\]](#)
22. Sundar, L.; Singh, M.; Sousa, A. Enhanced heat transfer and friction factor of MWCNT–Fe₃O₄/water hybrid nanofluids. *Int. Commun. Heat Mass Transf.* **2014**, *52*, 73–83. [\[CrossRef\]](#)
23. Dinarvand, S.; Rostami, M.N.; Dinarvand, R.; Pop, I. Improvement of drug delivery micro-circulatory system with a novel pattern of CuO–Cu/blood hybrid nanofluid flow towards a porous stretching sheet. *Int. J. Numer. Methods Heat Fluid Flow* **2019**, *29*, 4408–4429. [\[CrossRef\]](#)
24. Chahrehgh, H.S.; Dinarvand, S. TiO₂–Ag/blood hybrid nanofluid flow through an artery with applications of drug delivery and blood circulation in the respiratory system. *Int. J. Numer. Methods Heat Fluid Flow* **2020**, *30*, 4775–4796. [\[CrossRef\]](#)
25. Ramadhan, A.; Azmi, W.; Mamat, R.; Hamid, K. Experimental and numerical study of heat transfer and friction factor of plain tube with hybrid nanofluids, Case Stud. *Therm. Eng.* **2020**, *22*, 100782. [\[CrossRef\]](#)
26. Kim, T.; Li, Q.Z.J.; Jokerst, L.Z.J.V. A Gold/Silver Hybrid Nanoparticle for Treatment and Photoacoustic Imaging of Bacterial Infection. *ACS Nano* **2018**, *12*, 5615–5625. [\[CrossRef\]](#)
27. Rathore, N. A modified thermal flux model to examine the enhanced heat transmission in hybrid blood flow through artery: A comparison between Maxwell and Oldroyd-B models. *Proc. Inst. Mech. Eng. Part E J. Proc. Mech. Eng.* **2022**, 09544089221128367. [\[CrossRef\]](#)
28. Sandeep, N.; Samrat, S.; Ashwinkumar, G. Flow and heat transfer in radiative MHD dusty-hybrid ferrofluids. *Waves Random Complex Media* **2022**, 1–4. [\[CrossRef\]](#)
29. Rathore, N. Darcy–Forchheimer and Ohmic heating effects on GO–TiO₂ suspended cross nanofluid flow through stenosis artery. *Proc. Inst. Mech. Eng. Part C J. Mech. Eng. Sci.* **2022**, *236*, 09544062221105166. [\[CrossRef\]](#)

30. Riahi, M.K.; Ali, M.; Addad, Y.; Abu-Nada, E. Combined Newton–Raphson and Streamlines-Upwind Petrov–Galerkin iterations for nanoparticles transport in buoyancy-driven flow. *J. Eng. Math.* **2022**, *132*, 1–26. [[CrossRef](#)]
31. Durgaprasad, P.; Varma, S.V.; Hoque, M.M.; Raju, C.S. Combined effects of Brownian motion and thermophoresis parameters on three-dimensional (3D) Casson nanofluid flow across the porous layers slendering sheet in a suspension of graphene nanoparticles. *Neural Comput. Appl.* **2019**, *31*, 6275–6286. [[CrossRef](#)]
32. Wakif, A.; Animasaun, I.L.; Narayana, P.S.; Sarojamma, G. Meta-analysis on thermo-migration of tiny/nano-sized particles in the motion of various fluids. *Chin. J. Phys.* **2020**, *68*, 293–307. [[CrossRef](#)]
33. Amidu, M.A.; Addad, Y.; Riahi, M.K.; Abu-Nada, E. Numerical investigation of nanoparticles slip mechanisms impact on the natural convection heat transfer characteristics of nanofluids in an enclosure. *Sci. Rep.* **2021**, *11*, 1–24. [[CrossRef](#)] [[PubMed](#)]
34. Ijaz, S.; Iqbal, Z.; Maraj, E.; Nadeem, S. Investigation of Cu-CuO/blood mediated transportation in stenosed artery with unique features for theoretical outcomes of hemodynamics. *J. Mol. Liq.* **2018**, *254*, 421–432. [[CrossRef](#)]
35. Qureshi, M.Z.; Ali, K.; Iqbal, M.; Ashraf, M.; Ahmad, S. Heat and mass transfer enhancement of nanofluids flow in the presence of metallic/metallic-oxides spherical nanoparticles. *Eur. Phys. J. Plus* **2017**, *132*, 1–2. [[CrossRef](#)]
36. Sadiq, M.; Bahaidarah, H. Numerical Study on Generalized Heat and Mass in Casson Fluid with Hybrid Nanostructures. *Nanomaterials* **2021**, *11*, 2675. [[CrossRef](#)]
37. Alghamdi, W.; Alsubie, A.; Kumam, P.; Saeed, A.; Gul, T. MHD hybrid nanofluid flow comprising the medication through a blood artery. *Sci. Rep.* **2021**, *11*, 11621. [[CrossRef](#)]
38. Qureshi, M.Z.; Raza, Q.; Ramzan, A.; Faisal, M.; Ali, B.; Shah, N.A.; Weera, W. Activation Energy Performance through Magnetized Hybrid Fe₃O₄–PP Nanofluids Flow with Impact of the Cluster Interfacial Nanolayer. *Mathematics* **2022**, *9*, 3277. [[CrossRef](#)]
39. Rathore, N.; Sandeep, N. A relative study on blood-based cross ferrofluid flow over a stenosis artery. *Waves Random Complex Media* **2022**, *14*, 1–20. [[CrossRef](#)]
40. Maxwell, J. *A Treatise on Electricity and Magnetism*; Clarendon Press: Oxford, UK, 1873; Volume 1.
41. Hamilton, R.; Crosser, O. Thermal conductivity of heterogeneous two-component systems. *Ind. Eng. Chem. Fundam.* **1962**, *1*, 187–191. [[CrossRef](#)]
42. Qureshi, M.Z.; Bilal, S.; Chu, Y.M.; Farooq, A.B. Physical impact of nano-layer on nano-fluid flow due to dispersion of magnetized carbon nano-materials through an absorbent channel with thermal analysis. *J. Mol. Liq.* **2021**, *325*, 115211. [[CrossRef](#)]

Disclaimer/Publisher’s Note: The statements, opinions and data contained in all publications are solely those of the individual author(s) and contributor(s) and not of MDPI and/or the editor(s). MDPI and/or the editor(s) disclaim responsibility for any injury to people or property resulting from any ideas, methods, instructions or products referred to in the content.